Available online at www.sciencedirect.com
ScienceDirect
Trans. Nonferrous Met. Soc. China 34(2024) 2153−2166
Transactions of Nonferrous Metals Society of China
www.tnmsc.cn

Fabrication of Al coating for corrosion protection of Mg−Zn−Al−Sn−Mn alloy based on cold spraying process

Liang CHEN, Yi-hao BAO, Zhi-gang LI, Li-hua QIAN, Guo-qun ZHAO, Cun-sheng ZHANG

Key Laboratory for Liquid−Solid Structural Evolution and Processing of Materials (Ministry of Education), Shandong University, Jinan 250061, China

Received 31 January 2023; accepted 9 June 2023

Abstract: Al coating was fabricated on the surface of Mg−Zn−Al−Sn−Mn alloy by cold spraying process to enhance its corrosion resistance. The effects of temperature and pressure of working gas on the microstructure and corrosion behaviors of Al coating were investigated. The results show that as gas temperature and pressure increase, the densification and thickness of Al coating obviously increase. High gas temperature declines the critical velocity of powder deposition and increases the deposition efficiency. High gas pressure not only improves the quality of mechanical bonding, but also provides strong tamping effect on the deposited coating. Due to the reduction of porosity, the corrosion resistance of Al coating is improved with the increase of gas temperature and pressure. The corrosion products of $Al(OH)_3$ and Al_2O_3 can block the pores in Al coating and act as physical barriers to corrosion, which effectively protects Mg alloy from being corroded.

Key words: cold spraying; Mg alloy; Al coating; corrosion resistance; microstructure

1 Introduction

In order to reduce the energy consumption, the lightweight structural materials have been widely applied in the fields of automobile, high speed train and aircraft [1−3]. As the lightest structural metallic materials, Mg alloys have the advantages of low density, high specific strength, and high specific stiffness [4,5], and exhibit great potential in replacing steels and Al alloys.

Currently, there are still many problems hindering the engineering application of Mg alloys, among which the poor corrosion resistance is a primary one [6]. Lots of efforts have been devoted to overcoming the poor corrosion resistance of Mg alloys. LI et al [7] enhanced the corrosion resistance of Mg−0.6Al−0.5Mn−0.25Ca alloy by adding trace Ce. LONG et al [8] studied the effects of friction stir processing on the microstructure and corrosion resistance of as-cast Mg−5Zn−0.3Ca alloy, and found that the precipitate fragmentation weakened the galvanic corrosion. CHEN et al [9] reported that the annealing treatment effectively improved the corrosion resistance of hot-rolled AZ31 Mg by increasing the grain size and decreasing the numbers of dislocations and second phase particles, and high annealing temperature or long holding time could further reduce the corrosion rate.

Although the aforementioned methods can enhance the corrosion resistance of Mg alloys to a certain extent, the corrosion resistance of the finally obtained Mg alloys is still at a relatively low level. First of all, Mg alloys are more prone to galvanic corrosion with intermetallic compounds or other metallic elements [10]. Secondly, there is no film to protect Mg matrix from being corroded during corrosion [11]. Cold spraying is a process of

Corresponding author: Liang CHEN, Tel: +86-531-81696577, E-mail: chenliang@sdu.edu.cn;
Zhi-gang LI, Tel: +86-13127137256, E-mail: 201813761@mail.sdu.edu.cn
DOI: 10.1016/S1003-6326(24)66531-3

accelerating the spraying powders to impact the substrate at a relatively low temperature [12]. The tamping effect of the high-speed powder collision makes the cold-sprayed coating have the characteristic of low porosity [13]. Al has excellent corrosion resistance, and the driving force of galvanic corrosion between Mg and Al is low [14]. TAO et al [15] prepared pure Al coating on AZ91D Mg alloy through cold spraying, and revealed that the cold-sprayed Al coating exhibited good pitting corrosion resistance. DEFORCE et al [16] fabricated Al−5Mg coating by cold spraying to address the poor corrosion resistance of ZE41A-T5 Mg alloy. SIDDIQUE et al [17] prepared 6061 Al coating via cold spraying on AZ91D Mg substrate, and found that the coating with low porosity greatly improved the corrosion resistance of the substrate.

The temperature and pressure of gas are the key parameters of cold spraying process, and they have significant influence on the quality of the sprayed coating and the corrosion resistance of Mg alloys. In this study, the Al coating was fabricated on the surface of Mg−Zn−Al−Sn−Mn (ZATM6530) alloy by cold spraying method. The microstructure and corrosion behaviors of Al coatings with different process parameters were investigated. The effects of process parameters on the microstructure and corrosion behavior of the cold-sprayed Al coating were clarified, and the cold spraying parameters were optimized to achieve a good corrosion resistance of ZATM6530 Mg alloy.

2 Experimental

2.1 Materials

The ZATM6530 plate (Mg−6Zn−5Al−3Sn−0.3Mn, wt.%) with a thickness of 3 mm processed by hot extrusion, solution treatment, and peak aging was used as the substrate. The detailed procedures of hot extrusion can be found in recent study [18]. The solution treatment was carried out at 400 °C for 2 h, and then the samples were aged at 180 °C for 24 h to realize a peak-aging state. Afterwards, the substrate surface was ground using 2000# SiC paper to remove the impurities and oxide films. The powders used for cold spraying were commercially pure Al powders (Changsha TIJO Metal Material Co. Ltd., purity >99 wt.%). As seen from Fig. 1, the Al powders had a round shape with a size of 30−50 μm. Prior to spraying, the Al powders were shaken in a three-dimensional powder mixer and then dried under vacuum at 60 °C for 12 h to improve the fluidity of the powders.

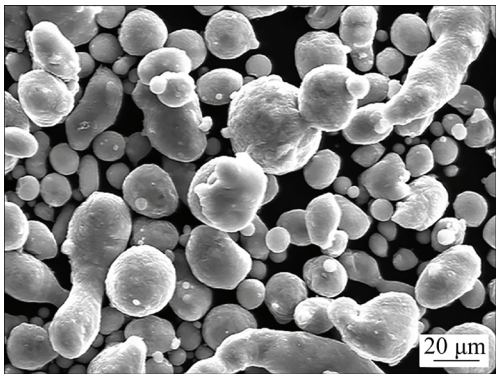

Fig. 1 Micro-morphology of Al powders

2.2 Cold spraying experiments

The portable cold spraying equipment (P800Q2-II) was employed, and the principle is schematically shown in Fig. 2(a). The equipment is mainly composed of nozzle, powder feeding device, powder mixer, gas heating device, gas source, and other auxiliary devices. In order to ensure the precise and smooth operation of the nozzle, the cold spraying equipment was equipped with a KUKA six-axis industrial robot arm (KR 600 R2830). The trajectory of the nozzle during the cold spraying experiment is drawn in Fig. 2(b).

The coating performance is mainly affected by the type of working gas, gas temperature, and gas

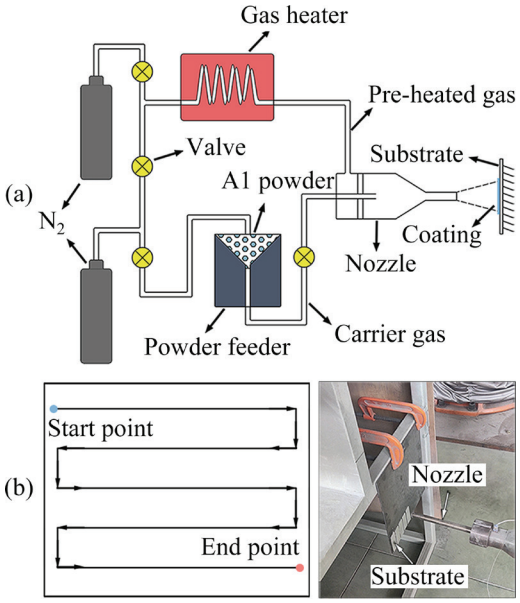

Fig. 2 Schematic diagram of cold spraying system (a) and trajectory of nozzle (b)

pressure. In this study, the compressed nitrogen was used as working gas, and the feed rate, spray distance, and lateral moving speed of nozzle were kept constant at 1.5 g/min, 20 mm, and 0.05 m/s, respectively. Four groups of experiments were carried out to study the effects of gas temperature and pressure on the microstructure and corrosion resistance of Al coating. The processing parameters of cold spraying experiments are listed in Table 1.

Table 1 Processing parameters of cold spraying experiments

Sample	Gas temperature/°C	Gas pressure/MPa
GT400-1.5	400	1.5
GT450-1.5	450	1.5
GT500-1.5	500	1.5
GT450-1.7	450	1.7

2.3 Microstructure characterization

The optical microscope (OM, DM6 M, Leica), scanning electron-microscope (SEM, JSM-7800F, JEOL), and X-ray diffraction (XRD, D8 discover, Bruker) were used to observe the surface morphology and microstructure of Al coating. The samples for microstructure analysis were firstly wet ground by silicon carbide papers from 800 to 2500 grit, and then polished by a mixture of 1.5 μm diamond suspension and oxide polishing suspension. The corrosion morphology and product were analyzed by SEM, electron probe micro-analyzer (EPMA, JXA−8530F PLUS, JEOL), and X-ray photoelectron spectroscopy (XPS, AXIS SUPRA, SHIMADZU). XPS was recorded with an X-ray beam spot of 650 μm (Al K_α source) and an energy resolution of 0.44 eV. The obtained XPS results were fitted using the software of CasaXPS. Each binding energy was corrected by the amount required to shift C 1s peak from the measured value to the standard value of 284.8 eV. The porosity of Al coatings was measured by Archimedes method. Each sample was tested 5 times, and the average value was taken as the final porosity.

2.4 Corrosion tests

The corrosion resistance of Al coating was tested by using potentio-dynamic polarization and electrochemical impedance spectroscopy (EIS) in 0.1 mol/L NaCl aqueous solution at room temperature. The tests were carried out on a PARSTAT electrochemical workstation with a typical three electrode cell. A saturated calomel electrode was used as the reference, and a platinum plate was used as the counter electrode. The sample with an exposed surface area of 1 cm^2 served as working electrode. Each test was repeated 5 times to achieve a good reproducibility. Prior to potentio-dynamic measurement, the sample was immersed into NaCl solution for 30 min to stabilize at the open circuit potential (OCP). Afterwards, the potentio-dynamic polarization curves were recorded within the potential range of ±250 mV (vs OCP) with a scanning rate of 0.167 mV/s. The EIS was conducted over a frequency ranging from 100 kHZ to 0.1 Hz by using a 10 mV amplitude sinusoidal voltage after immersion in 0.1 mol/L NaCl solution for 0.5, 1, 2, 4, 8, 12, and 24 h. The experimental data were analyzed by using the commercial software of ZsimpWin.

3 Results and discussion

3.1 Microstructure of Al coating

Figure 3 plots the XRD patterns of Al powders and Al coatings prepared using different cold spraying parameters. It is seen that α(Al) is the primary phase in both Al powders and Al coatings. Besides, other diffraction peaks cannot be found in Fig. 3, indicating that the oxidation of Al powder and phase transition do not occur during the cold spraying process. Even if the oxidation occurs on the surface of deposited coating, the subsequent high-speed Al powders can immediately destroy the oxide film [19,20]. Therefore, it is concluded that

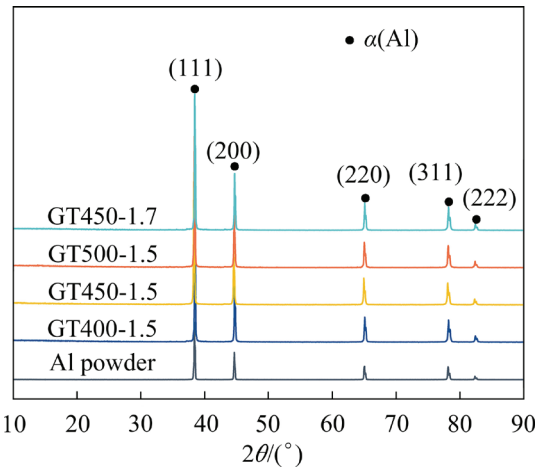

Fig. 3 XRD patterns of Al powders and as-sprayed Al coatings

cold spraying is effective in avoiding the oxidation of Al coating.

Figure 4 shows the three-dimensional surface morphologies of the Al coatings prepared using different processing parameters. It is clearly seen that all coatings have rough surfaces with large amount of island-like protrusions, and the undulation heights of the coatings are significantly different. By comparing Figs. 4(a−c), it is observed that the undulation heights of the coating surfaces are 242.19 μm at 400 °C and 170.34 μm at 500 °C, indicating a decreasing tendency with the increase of gas temperature. At 450 °C, as the gas pressure increases from 1.5 to 1.7 MPa, the undulation height of the coating surface decreases from 198.43 to 154.65 μm, as shown in Figs. 4(b, d). The above facts demonstrate that high gas temperature and pressure can reduce the roughness and improve the uniformity of the coating surface.

Figure 5 shows the optical morphologies of surfaces and cross-sections of Al coatings prepared using different process parameters. From the cross-sectional images of the coatings, it is seen that there is a clear interface between the coating and substrate, and all coatings exhibit obvious pores. Under the gas pressure of 1.5 MPa, a large number of pores exist in the coating when the gas temperature is 400 °C, and the cracks appear at the coating/substrate interface. When the gas temperature rises to 450 °C, the number of pores clearly decreases, but a certain number of small pores still exist at the coating/substrate interface. When the gas temperature further increases to 500 °C, the size and number of pores are obviously reduced, and the bonding quality of the interface is greatly improved. If the gas temperature is kept constant at 450 °C, as the gas pressure increases from 1.5 to 1.7 MPa, the number and size of pores are all significantly reduced. These facts agree well with the three-dimensional surface morphologies shown in Fig. 4.

Figure 6 presents the SEM images of Al coatings, and the calculated results of coating porosity and the measured results of coating thickness are listed in Table 2. Based on Fig. 6 and Table 2, it is clearly seen that when the gas temperature increases from 400 to 500 °C, the porosity of Al coating gradually decreases. The reason is that high gas temperature reduces the critical velocity of powder deposition and increases the deposition efficiency of Al powder [21], causing an improvement of coating densification. When the gas pressure increases from 1.5 to 1.7 MPa, the coating porosity also significantly decreases. It is known that high gas pressure can increase the impact force of powder on the substrate or the deposited coating. The higher impact force is beneficial to achieving a better mechanical bonding

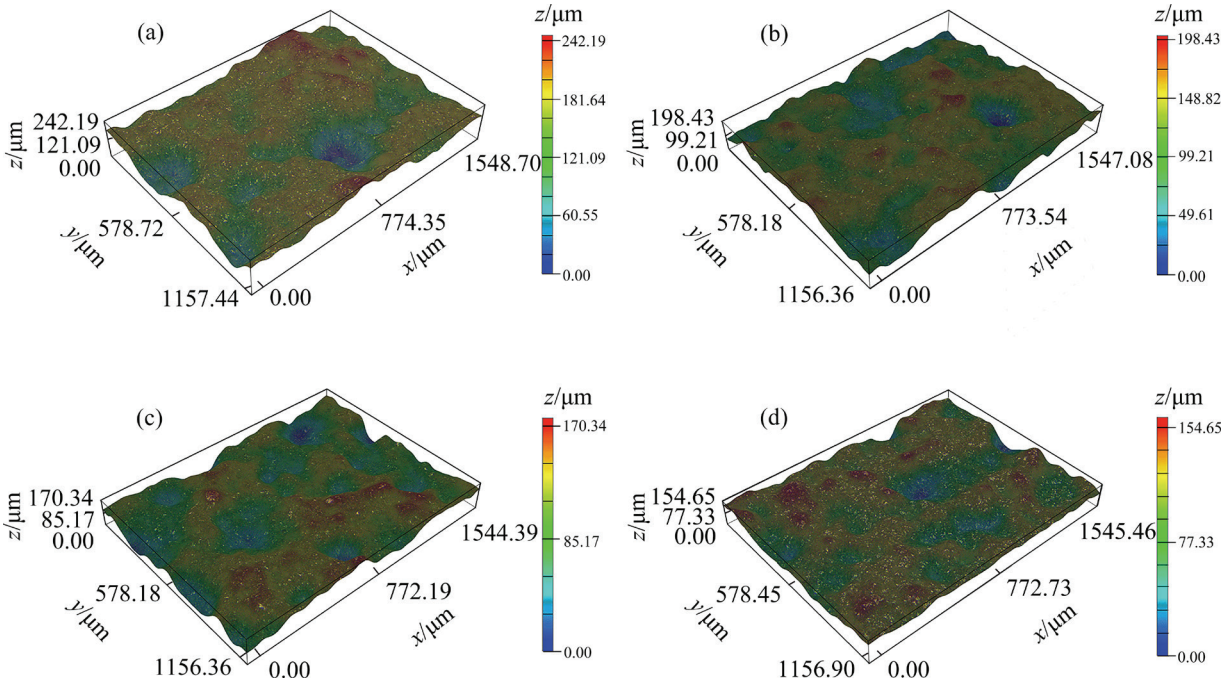

Fig. 4 Three-dimensional morphologies of Al coatings: (a) GT400-1.5; (b) GT450-1.5; (c) GT500-1.5; (d) GT450-1.7

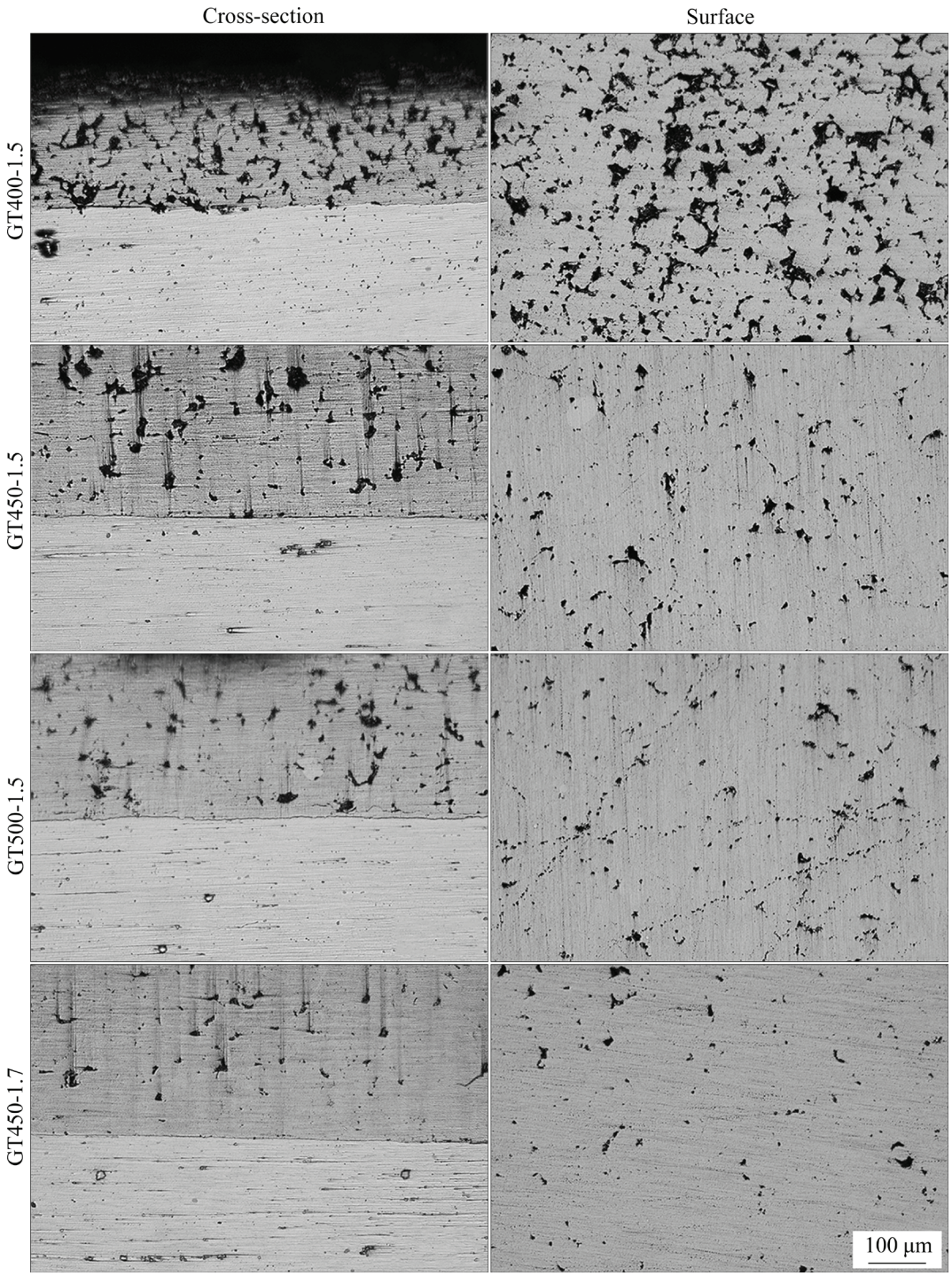

Fig. 5 Optical morphologies of cross-sections and surfaces of Al coatings

between Al powder and the substrate or between Al powder and the deposited coating. On the other hand, higher impact force provides a tamping effect on the deposited coating [22,23]. As a result, the densification of Al coating increases with the increase of gas pressure.

The thickness of Al coating varies with the gas temperature and pressure, and the measured values are listed in Table 2. It is clear that the coating thickness increases significantly with the increase of gas temperature. The average thickness is only 418.7 μm, when the gas temperature is 400 °C. As the gas temperature rises to 450 and 500 °C, the average thickness increases to 555.2 and 754.6 μm, and the corresponding amplifications are 32.6% and 80.2%, respectively. The above facts indicate that

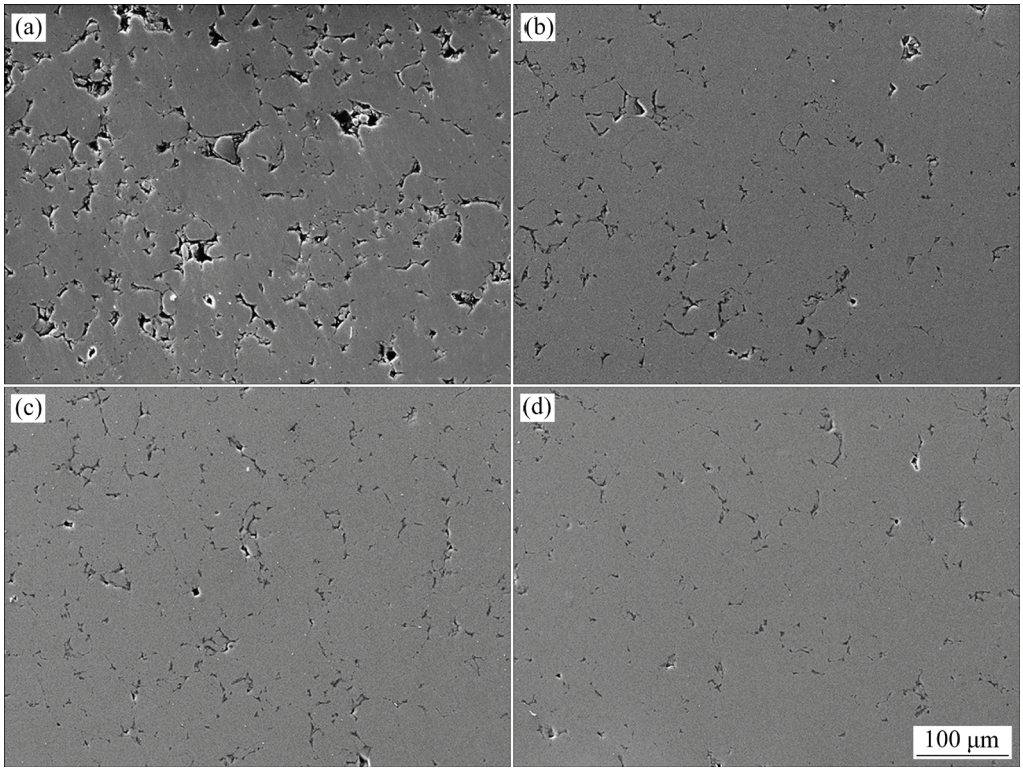

Fig. 6 SEM images of Al coatings: (a) GT400-1.5; (b) GT450-1.5; (c) GT500-1.5; (d) GT450-1.7

Table 2 Porosity and thickness of Al coatings prepared with different processing parameters

Sample	Porosity/%	Thickness/μm
GT400-1.5	4.73±0.32	418.7±26.3
GT450-1.5	1.67±0.26	555.2±34.5
GT500-1.5	1.24±0.19	754.6±16.8
GT450-1.7	0.97±0.15	788.3±28.9

the deposition efficiency of Al powders is enhanced by increasing the gas temperature. By comparing GT450-1.5 with GT450-1.7, it is seen that when working gas temperature is constant at 450 °C, high gas pressure can improve the deposition efficiency of Al powders, which in turn increases the coating thickness.

Figure 7 displays the SEM images of the cross-sections of Al coatings. It is observed from Figs. 7(a, c, e) that the coating near coating/substrate interface is denser and less porous than the coating surface. This phenomenon should be related to the mechanical bonding mechanisms originating from the following aspects. First of all, Al has a face-centered cubic crystal structure with many slip systems, and it deforms easily under the action of external forces. When Al powders with a high speed impact the substrate surface or the previously deposited coating surface, high stress and strain can be generated [21,24]. As a result, the depressions or micropores on the previously deposited coating surface are filled with the severely deformed Al powders, which in turn improves the mechanical bonding of the coating/substrate interface. On the other hand, not all Al powders are deposited during cold spraying process, and some of them are bounced back by the coating. These powders also exert tamping effects on the deposited coating, resulting in a better mechanical bonding. Hence, the lower frequency of subsequent powder impacts and the smaller tamping effect cause a higher porosity in the area near the coating surface [25]. The similar phenomenon can be found in the cold spraying of nano-5083Al powders reported by AJDELSZTAJN et al [26]. There are almost no defects near the coating/substrate interface, while the cracks exist in the area near the coating surface. Moreover, it is observed from Figs. 7(b, d, f, h) that the coating/substrate interface is clean with few holes and cracks. Hence, it is concluded that the Al coating has achieved good mechanical bonding with ZATM6530 Mg substrate.

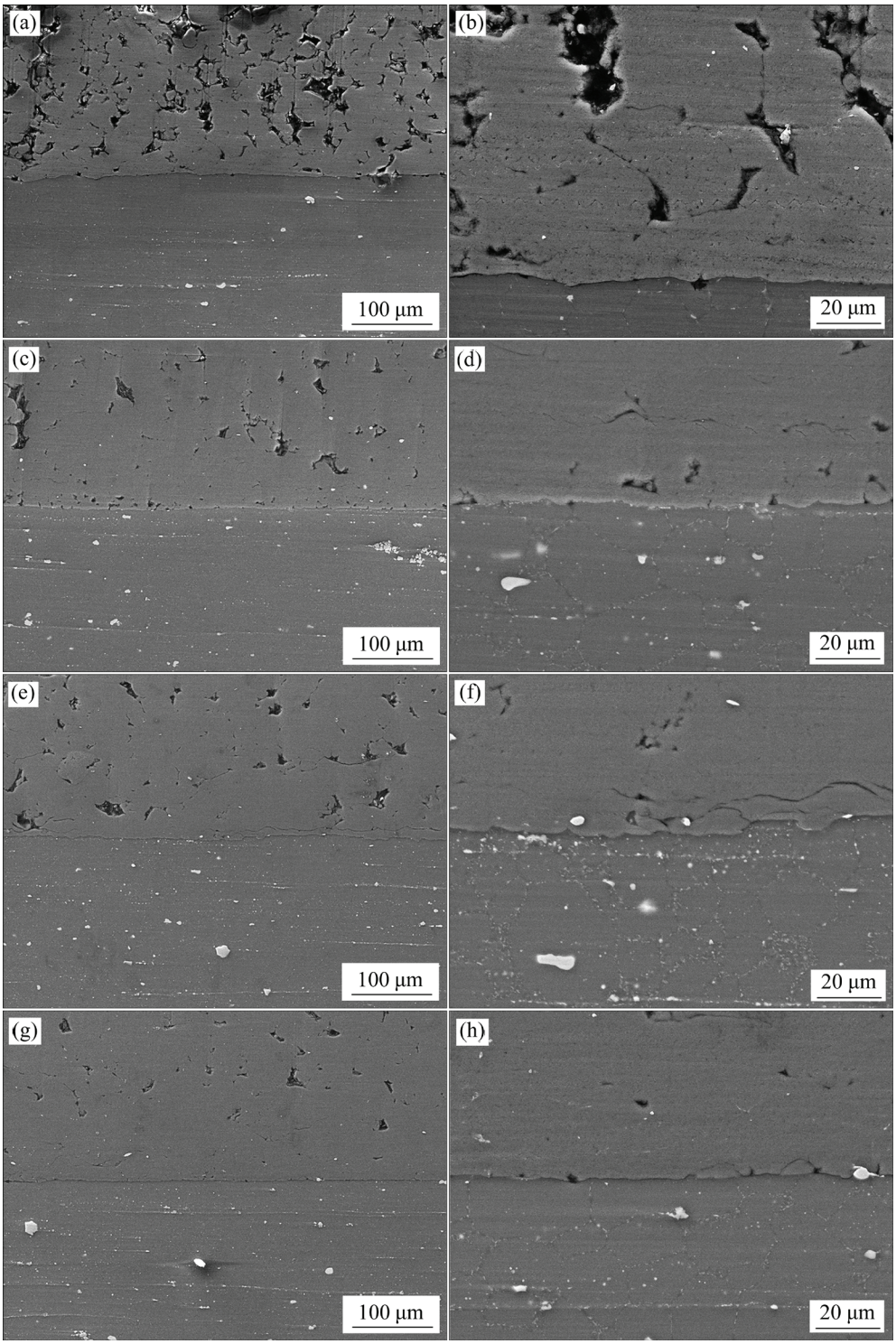

Fig. 7 SEM images of cross-sections of Al coatings: (a, b) GT400-1.5; (c, d) GT450-1.5; (e, f) GT500-1.5; (g, h) GT450-1.7

3.2 Corrosion behavior of Al coatings

The potentio-dynamic polarization curves tested in 0.1 mol/L NaCl solution of the Al coatings are plotted in Fig. 8. The corresponding corrosion parameters obtained based on cathodic Tafel extrapolation are listed in Table 3. As seen from Fig. 8, except for Sample GT400-1.5, the potentio-dynamic polarization curves of the other samples all show an obvious passivation trend. It is proven that the oxidation of Al generates a relatively dense oxide or hydroxide film on the coating surface, which can prevent the corrosion from extending

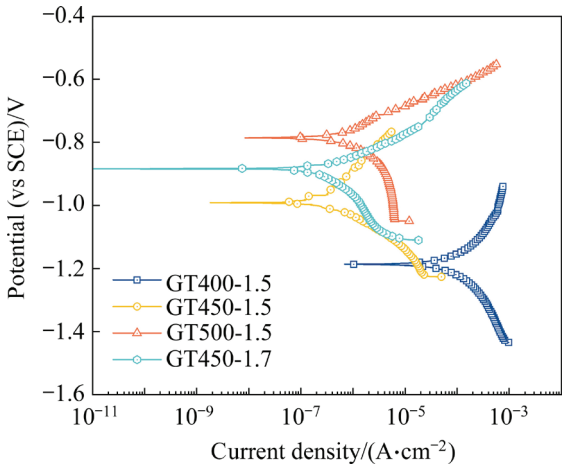

Fig. 8 Potentio-dynamic polarization curves of Al coatings

Table 3 Corrosion parameters of Al coatings derived from potentio-dynamic polarization curves

Sample	φ_{corr} (vs SCE)/V	J_{corr}/(μA·cm^{-2})
GT400-1.5	−1.187	63.088
GT450-1.5	−0.991	0.318
GT500-1.5	−0.786	0.435
GT450-1.7	−0.885	0.164

into the coating interior. It is seen from Fig. 8 and Table 3 that GT400-1.5 has high corrosion tendency and corrosion current density. When gas temperature rises to 450 °C, the corrosion potential of Al coating increases obviously, and the corrosion current density decreases by two orders of magnitude, indicating that the corrosion tendency and rate of Al coating decrease significantly. As gas temperature continues to rise to 500 °C, the corrosion tendency gradually decreases, while the corrosion rate increases slightly. This phenomenon may be attributed to the lower porosity and the larger effective contacting area with the corrosion solution of GT500-1.5, leading to a higher corrosion current density. However, the corrosion current density of GT500-1.5 has basically the same order of magnitude as that of GT450-1.5. These facts indicate that a high gas temperature causes a low corrosion tendency of Al coating and causes corrosion rate to decrease and gradually stabilize. As gas pressure rises from 1.5 to 1.7 MPa, the corrosion potential increases and the corrosion current density decreases, which demonstrates that the increase of gas pressure can reduce the tendency and rate of corrosion of Al coating. It has been mentioned that the densification of Al coating increases with the increase of gas temperature and pressure, which is consistent with the variation of corrosion tendency and rate. Hence, it is inferred that the densification of Al coating affects the corrosion resistance.

In order to study the corrosion resistance and corrosion kinetic transformation of Al coating after long-term immersion in NaCl solution, EIS analysis was conducted and the results are plotted in Fig. 9. As seen, except for GT400-1.5, the Nyquist curves of other Al coatings show a similar tendency, viz., with the extension of immersion time, the radius values of capacitive loops at high frequency firstly increase, then decrease and finally increase again. At the initial stage of immersion, the Nyquist curve of each Al coatings is composed of a capacitive loop at medium and high frequencies and a straight line at low frequency. The reason is that the Al coating is polished before the electrochemical impedance test, and the coating surface is smooth with low roughness. When the coating surface is exposed to the corrosive fluid, a thin oxide film is generated rapidly, and the infiltration rate of the corrosive solution is slowed down. With the prolongation of immersion time, the oxide film is gradually destroyed. Since a certain number of pores exist in Al coating, Cl^- gradually erodes the coating interior. As a result, the coating itself undergoes electrochemical corrosion dissolution, which in turn leads to a decrease of corrosion resistance. With the further extension of immersion time, except for GT400-1.5, the radii of capacitive loops of other Al coatings increase gradually, indicating that the corrosion products can block the pores in coating and act as physical barriers to prevent corrosion, thereby improving the corrosion resistance [27]. For GT400-1.5, it is seen from Fig. 9(a) that the radius of capacitive loop firstly increases and then decreases with the extension of immersion time, and the corrosion resistance is not enhanced at the later stage of immersion, which should be caused by its high porosity. Based on Figs. 6, 7, and Table 2, it is found that GT400-1.5 has large pore size and high porosity. It is difficult for corrosion products to form dense films to block the large pores in Al coating. Therefore, the corrosion resistance of GT400-1.5 during the immersion process is hard to be improved.

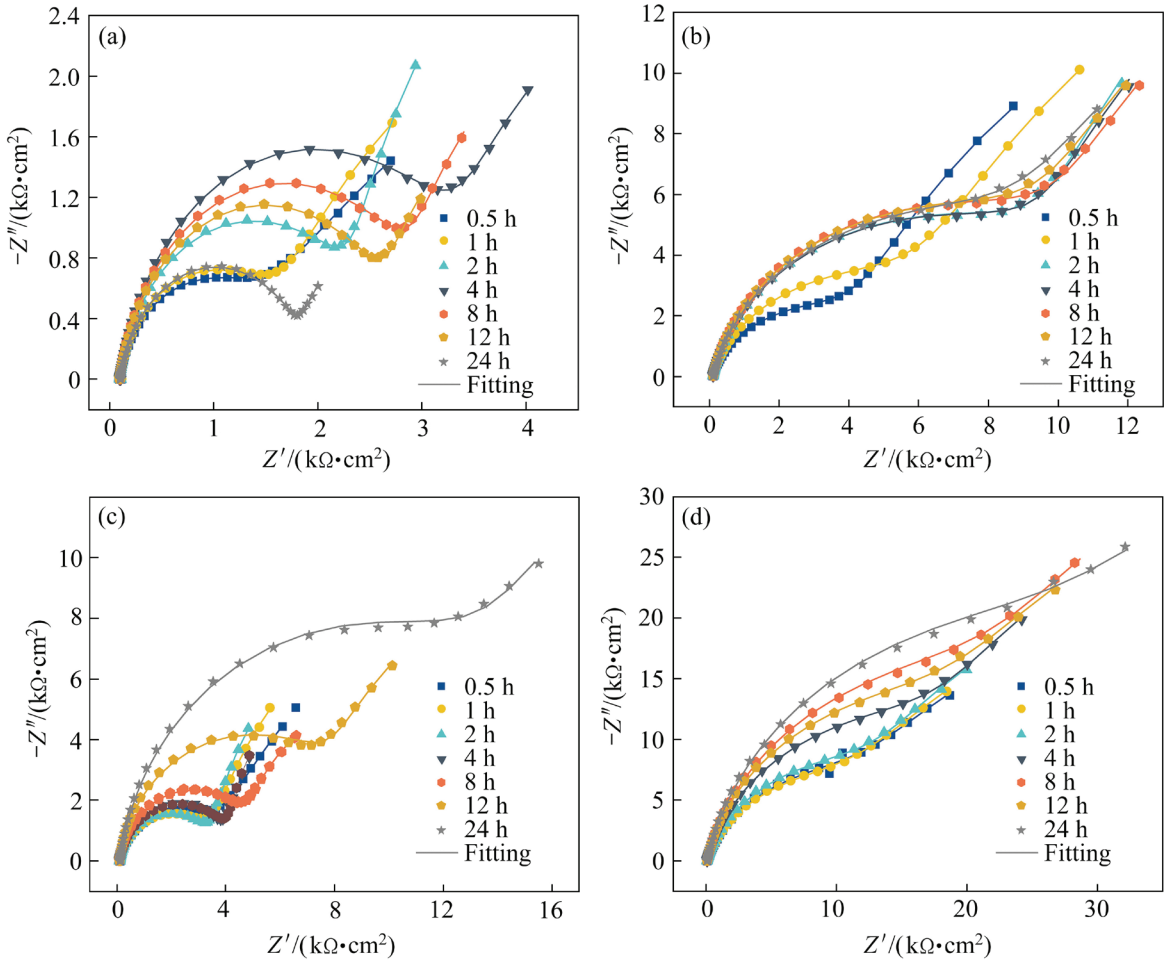

Fig. 9 Nyquist plots of Al coatings after immersion in NaCl solution for 0.5−24 h: (a) GT400-1.5; (b) GT450-1.5; (c) GT500-1.5; (d) GT450-1.7

In order to make a further investigation, the equivalent circuit model shown in Fig. 10(a) is adopted to fit the Nyquist curves. In the equivalent circuit, R_s represents the solution resistance, Q_c represents the capacitance of Al coating, R_{po} is the resistance of the pores in Al coating, Q_{dl} represents the double layer capacitance, and R_{ct} represents the charge transfer resistance. It is noted that Q contains two parameters of Y_0 and the dimensionless exponent n ($0<n<1$). This equivalent circuit is commonly used to fit the relatively dense Al coating [28], and its equivalent circuit model can be described as $R_s(Q_c(R_{po}(Q_{dl}R_{ct})))$. The polarization resistance R_p representing the corrosion resistance can be calculated based on the equation of $R_p=R_{po}+R_{ct}$. Accordingly, the results of R_p are shown in Fig. 10(b). R_p value is inversely proportional to the corrosion rate of the coating. A higher R_p value means a better corrosion resistance. It is seen that when the gas temperature increases from 400 to

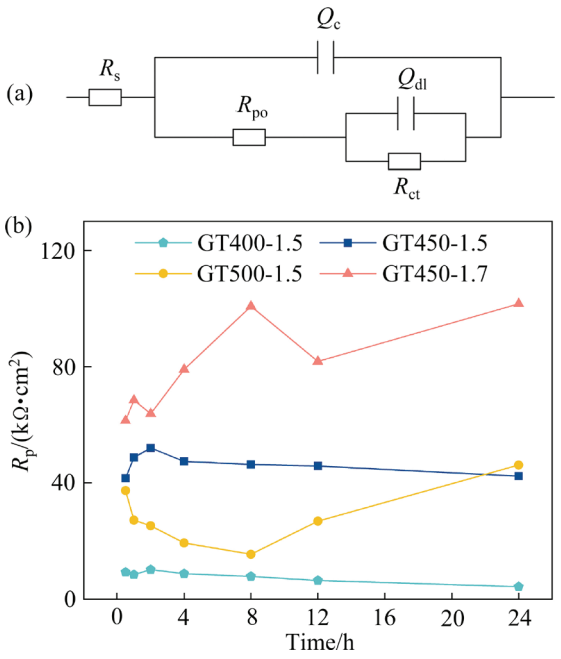

Fig. 10 Equivalent circuit for EIS data (a) and evolution of resistance R_p (b)

450 °C, R_p value greatly increases. Based on the microstructure differences of the coatings, it is known that the decrease of the porosity greatly improves the corrosion resistance. The R_p value of GT500-1.5 is lower than that of GT450-1.5 at the early stage of immersion, which may be related to the formation rate of corrosion products. However, after 24 h immersion, the corrosion resistance of GT500-1.5 is better than that of GT450-1.5. When the gas pressure increases from 1.5 to 1.7 MPa, the R_p value of the coating increases by an order of magnitude, and the corrosion resistance is remarkably improved. Moreover, from Fig. 10(b), it is also observed that the R_p value of GT400-1.5 is always the lowest, which further proves that the corrosion products of this coating cannot aggregate and block the pores to hinder the propagation of corrosion. The above results are consistent with those obtained from potentio-dynamic polarization.

According to the results of potentio-dynamic polarization tests and EIS analysis, it is known that the process parameters of cold spraying have significant influence on the corrosion resistance of Al coating. In order to study the actual corrosion mechanism of Al coating, the morphologies and products after immersion in 0.1 mol/L NaCl for 12 h were observed, as shown in Fig. 11. It is seen from Fig. 11(a) that the coating surface of GT400-1.5 has obvious corrosion cracks. Besides, a large number of corrosion products exist on the coating surface of GT400-1.5, while the corrosion products are not dense. Because of the high porosity and large pore size of the coating, the corrosion products cannot accumulate and block the pores, and it is difficult to prevent the propagation of corrosion. These facts are consistent with the EIS analysis of GT400-1.5. As shown in Fig. 11(b), when the gas temperature increases from 400 to 450 °C, the corrosion products generate a dense film, which can block and fill most of the defects on the coating surface, resulting in a better corrosion resistance. However, the dense film of corrosion products is not formed on the coating surface of GT500-1.5, and the corrosion resistance is not greatly improved, which agrees well with the results presented in Figs. 10 and 11. From Fig. 11(d), it is found that only the corrosion cracks with small size and few corrosion products appear on the coating surface of GT450-1.7. Combined with the low porosity of the coating, the oxide film generated by the dense Al coating after contacting with the corrosion solution resists the erosion of Cl^- during the long-time immersion, and thus the corrosion rate is slowed down. According to the EIS

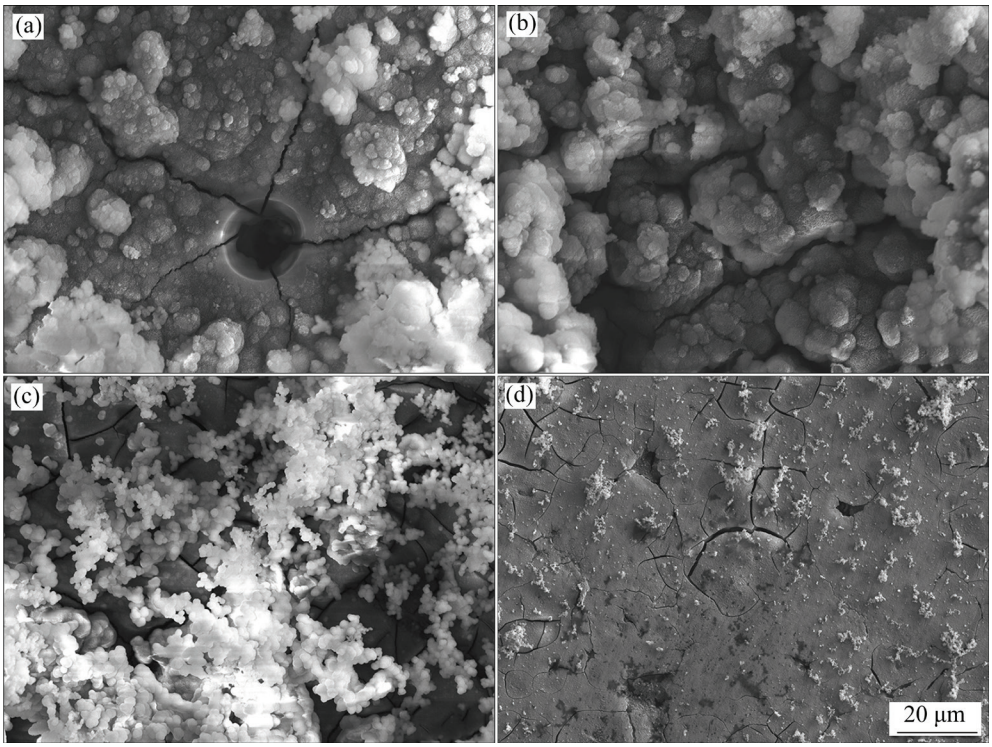

Fig. 11 Corrosion morphologies of Al coatings after immersion in 0.1 mol/L NaCl for 12 h: (a) GT400-1.5; (b) GT450-1.5; (c) GT500-1.5; (d) GT450-1.7

results, with the extension of immersion time, the corrosion resistance of the coating is further improved after the formation of dense corrosion product film.

With the purpose of analyzing the types of corrosion products, XPS and EPMA were adopted to characterize the corroded surface of Al coating. Since the corrosion products of all coatings are similar, only the XPS and EPMA results of GT500-1.5 are given. Figure 12 shows the XPS results of the corrosion products on the corroded surface of GT500-1.5, and Fig. 13 displays the EPMA image and distributions of the main elements. As seen from Fig. 12(a), the corrosion products are mainly composed of O and Al elements. The EPMA results shown in Fig. 13 also reveal the presence of O and Al. For the XPS data shown in Fig. 12(c), two characteristic peaks at 532.1 and 531.3 eV are obvious. These two peaks correspond to O^{2-} and OH^{-}, respectively, which can be used to determine the existence of oxides and hydroxides in the corrosion product layer. As shown in Fig. 12(d), by fitting the Al element spectra, it is indicated that the oxides and hydroxides in corrosion product layer are Al_2O_3 and $Al(OH)_3$, respectively. Since the corrosion products are relatively dense and insoluble in corrosive solution, they play a protective role in corrosion process and improve the corrosion resistance of the coating.

3.3 Effects of microstructure on corrosion resistance

The results of electrochemical tests and corrosion morphologies indicate that the corrosion resistance of Al coating with a fixed gas pressure is ranked as GT500-1.5 > GT450-1.5 > GT400-1.5. When gas temperature is constant, the corrosion resistance of GT450-1.7 is much better than that of GT450-1.5. Based on the previous studies [29−31], the long-term corrosion resistance of metal coating mainly depends on the porosity. As mentioned above, high gas temperature can reduce the critical velocity of powder deposition and increase the deposition efficiency, both of which are beneficial to improving the densification of coating. The high gas pressure can not only improve the mechanical bonding, but also exert strong tamping effects on the deposited coating. As a result, the densification of Al coating increases with the increase of gas pressure. When Al coating is exposed to corrosive

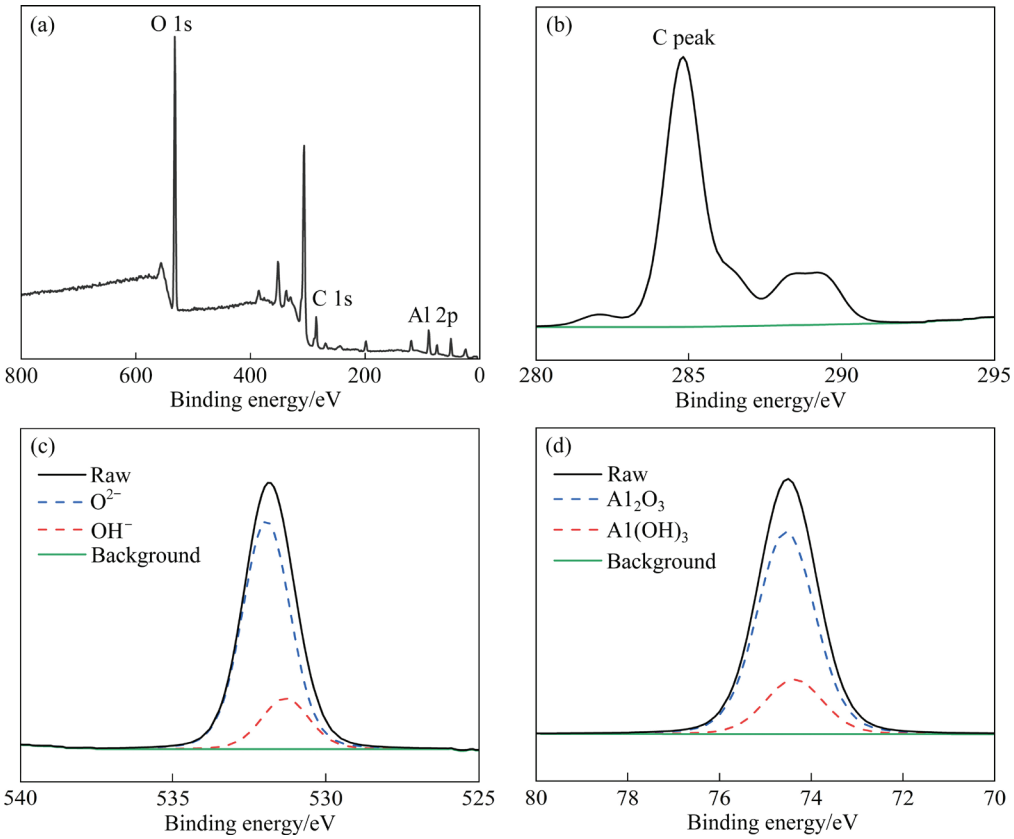

Fig. 12 XPS results of corrosion products on corroded surface of GT500-1.5: (a) Wide scan spectra; (b) C 1s; (c) O 1s; (d) Al 2p

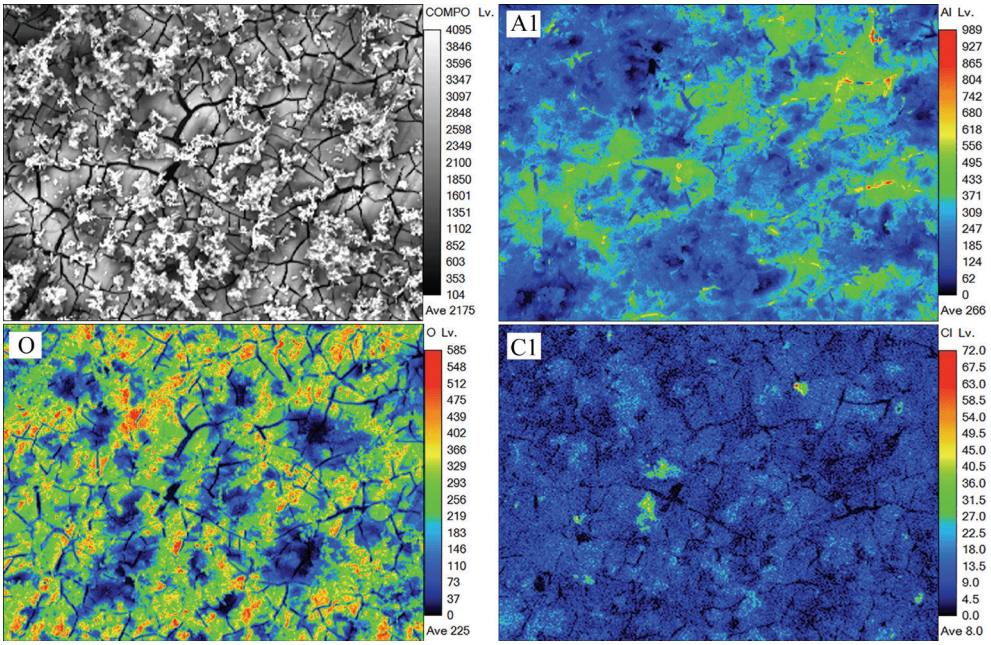

Fig. 13 EPMA images of GT500-1.5 and corresponding elemental distributions of Al, O, and Cl

media, a dense oxide film is formed on the coating surface with high densification, which is beneficial to enhancing the resistance of coating to erosion. Even if the oxide film is destroyed by Cl^-, the corrosion products can still accumulate in small pores or cracks in the dense coating and hinder the propagation of corrosion [32].

4 Conclusions

(1) High gas temperature reduces the critical velocity of powder deposition and increases the deposition efficiency. High gas pressure not only enhances the quality of mechanical bonding, but also provides strong tamping effect on the deposited coating. The densification and thickness of Al coating increase greatly with the increase of gas temperature and gas pressure.

(2) The corrosion resistance of Al coatings with a fixed gas pressure of 1.5 MPa is ranked as GT500-1.5 > GT450-1.5 > GT400-1.5. When the gas temperature is constant at 450 °C, the corrosion resistance of GT450-1.7 is much better than that of GT450-1.5. The corrosion resistance of Al coating is mainly affected by porosity, and the denser the coating, the better the corrosion resistance. The corrosion products of $Al(OH)_3$ and Al_2O_3 can block the pores in the coating and act as physical barriers to prevent the corrosion.

CRediT authorship contribution statement

Liang CHEN: Investigation, Conceptualization, Methodology, Funding acquisition, Writing − Original draft; **Yi-hao BAO:** Conceptualization, Data curation, Investigation, Writing − Original draft; **Zhi-gang LI:** Data curation, Investigation, Validation; **Li-hua QIAN:** Data curation, Investigation; **Guo-qun ZHAO:** Supervision, Resources, Writing − Review & editing; **Cun-sheng ZHANG:** Writing − Review & editing.

Declaration of competing interest

The authors declare that they have no known competing financial interests or personal relationships that could have appeared to influence the work reported in this paper.

Acknowledgments

The authors would like to acknowledge the financial support from the National Natural Science Foundation of China (No. 52222510), and Key Research and Development Program of Shandong Province, China (No. 2021ZLGX01).

References

[1] ZHAO Jun, JIANG Bin, SONG Yan, DAI Zuo-cai, LU Li-wei, HE Chao, HUANG Guang-sheng, ZHANG Ding-fei, PAN Fu-sheng. Simultaneous improvement of strength and ductility by Mn addition in extruded Mg−Gd−Zn alloy [J]. Transactions of Nonferrous Metals Society of China, 2022, 32(5): 1460−1471.

[2] CHRISTY J V, MOURAD A H I, SHERIF M M,

SHIVAMURTHY B. Review of recent trends in friction stir welding process of aluminum alloys and aluminum metal matrix composites [J]. Transactions of Nonferrous Metals Society of China, 2021, 31(11): 3281−3309.

[3] ZHANG Yi, FENG Xiao-hui, HUANG Qiu-yan, LI Ying-ju, YANG Yuan-sheng. Enhancing mechanical properties and degradation performance of Mg−0.8wt.%Ca alloy by directional solidification [J]. Transactions of Nonferrous Metals Society of China, 2023, 33(2): 409−421.

[4] TANG Jian-wei, CHEN Liang, LI Zhi-gang, ZHAO Guo-qun, ZHANG Cun-sheng, ZUO Yang. Evolution mechanisms of charge weld during porthole die extrusion of ZK60 Mg profile [J]. Journal of Materials Processing Technology, 2022, 300: 117401.

[5] CHEN Liang, CHENG Qian, TANG Jian-wei, LI Zhi-gang, ZHAO Guo-qun, ZUO Yang. Numerical and experimental study on extrusion of ZK60 Mg alloy using billet with temperature gradient [J]. Journal of Materials Research and Technology, 2021, 14: 3018−3028.

[6] BAHMANI A, LOTFPOUR M, TAGHIZADEH M, KIM W J. Corrosion behavior of severely plastically deformed Mg and Mg alloys [J]. Journal of Magnesium and Alloys, 2022, 10: 2607−2648.

[7] LI Mei-Xuan, WANG Cheng, LI Yi-Jia, WANG Da-Wei, ZHA Min, GAO Yi-peng, WANG Hui-Yuan. Tailoring the microstructure and enhancing the corrosion resistance of extruded dilute Mg−0.6Al−0.5Mn−0.25Ca alloy by adding trace Ce [J]. Corrosion Science, 2022, 207: 110605.

[8] LONG Fei, LIU Qu, CHEN Gao-qiang, ZHOU Meng-ran, SHI Qing-yu. Improved corrosion resistance achieved in a friction stir processed Mg−5Zn−0.3Ca alloy with fragmented precipitates [J]. Corrosion Science, 2022, 208: 110675.

[9] CHEN Hao, TANG Jian-wei, GONG Wei-wei, GAO Yun-peng, TIAN Feng, CHEN Liang. Effects of annealing treatment on the microstructure and corrosion behavior of hot rolled AZ31 Mg alloy [J]. Journal of Materials Research and Technology, 2021, 15: 4800−4812.

[10] XIE Jin-shu, ZHANG Jing-huai, ZHANG Zhi, QIU Xin, ZHANG Hao, ZHANG Hao-dong, JIAO Xing-kai, WU Xiao-han, WU Rui-zhi. Corrosion behavior and mechanism of Mg−Er−Zn−Zr alloys in different states [J]. Journal of Materials Research and Technology, 2022, 19: 30−45.

[11] URA-BINCZYK E, HOMAZAVA N, ULRICH A, HAUERT R, LEWANDOWSKA M, KURZYDLOWSKI K J, SCHMUTZ P. Passivation of Al−Cr−Fe and Al−Cu−Fe−Cr complex metallic alloys in 1 M H_2SO_4 and 1 M NaOH solutions [J]. Corrosion Science, 2011, 53: 1825−1837.

[12] ASSADI H, KREYE H, GAERTNER F, KLASSEN T. Cold spraying—A materials perspective [J]. Acta Materialia, 2016, 116: 382−407.

[13] STOLTENHOFF T, BORCHERS C, GARTNER F, KREYE H. Microstructures and key properties of cold-sprayed and thermally sprayed copper coatings [J]. Surface & Coatings Technology, 2006, 200: 4947−4960.

[14] LI Zhi-gang, CHEN Liang, TANG Jian-wei, ZHAO Guo-qun, ZHANG Cun-sheng, CHU Xing-rong. Microstructure evolution, plastic anisotropy, and intergranular corrosion of Al−Mg−Si sheet processed through a combination of hot extrusion and cold rolling [J]. Materials Characterization, 2020, 164: 110299.

[15] TAO Yong-shan, XIONG Tian-ying, SUN Chao, KONG Ling-yan, CUI Xin-yu, LI Tie-fan, SONG Guang-Ling. Microstructure and corrosion performance of a cold sprayed aluminium coating on AZ91D magnesium alloy [J]. Corrosion Science, 2010, 52: 3191−3197.

[16] DEFORCE B S, Eden T J, POTTER J K. Cold spray Al−5%Mg coatings for the corrosion protection of magnesium alloys [J]. Journal of Thermal Spray Technology, 2011, 20: 1352−1358.

[17] SIDDIQUE S, LI Cheng-xin, BERNUSSI A A, HUSSAIN S W, YASIR M. Enhanced electrochemical and tribological properties of AZ91D magnesium alloy via cold spraying of aluminum alloy [J]. Journal of Thermal Spray Technology, 2019, 28: 1739−1748.

[18] BAO Yi-hao, CHEN Liang, TANG Jian-wei, LI Zhi-gang, ZHAO Guo-qun, ZHANG Cun-sheng. Investigation on corrosion behavior and mechanical properties of an extruded Mg−Zn−Al−Sn−Mn alloy [J]. Materials Characterization, 2021, 180: 111439.

[19] NAVABI A, VANDADI M, BOND T, RAHNESHIN V, OBAYEMI J, AHMED R, OGHENEVWETA J E, CHAMPAGNE V, RAHBAR N, SOBOYEJO W O. Deformation and cracking phenomena in cold sprayed 6061 Al alloy powders with nanoscale aluminum oxide films [J]. Materials Science and Engineering A, 2022, 841: 143036.

[20] HEMEDA A A, ZHANG C, HU X, FUKUDA D, COTE D, NAULT I M, NARDI A, CHAMPAGNE V K, MA Y, PALKO J W. Particle-based simulation of cold spray: Influence of oxide layer on impact process [J]. Additive Manufacturing, 2021, 37: 101517.

[21] ASSADI H, GARTNER F, STOLTENHOFF T, KREYE H. Bonding mechanism in cold gas spraying [J]. Acta Materialia, 2003, 51: 4379−4394.

[22] van STEENKISTE T H, SMITH J R, TEETS R E. Aluminum coatings via kinetic spray with relatively large powder particles [J]. Surface & Coatings Technology, 2002, 154: 237−252.

[23] MANAP A, MAHALINGAM S, YUSOF S N A, AFANDI N, ABDULLAH H. Impact behaviour of aluminum particles upon aluminum, magnesium, and titanium substrates using high pressure and low-pressure cold spray [J]. Sains Malaysiana, 2022, 51: 585−597.

[24] LIU Tian, LEAZER J D, BREWER L N. Particle deformation and microstructure evolution during cold spray of individual Al−Cu alloy powder particles [J]. Acta Materialia, 2019, 168: 13−23.

[25] WATHANYU K, TUCHINDA K, DAOPISET S, SIRIVISOOT S. Corrosion resistance and biocompatibility of cold-sprayed titanium on 316L stainless steel [J]. Surface & Coatings Technology, 2022, 445: 128721.

[26] AJDELSZTAJN L, JODOIN B, KIM G E, SCHOENUNG J M. Cold spray deposition of nanocrystalline aluminum alloys [J]. Metallurgical and Materials Transactions A, 2005, 36: 657−666.

[27] ZHANG L M, ZHANG S D, Ma A L, HU H X, ZHENG Y G, YANG B J, WANG J Q. Influence of sealing treatment on the corrosion behavior of HVAF sprayed Al-based amorphous/ nanocrystalline coating [J]. Surface & Coatings Technology,

2018, 353: 263−273.

[28] LOPEZ-ORTEGA A, ARANA J L, RODRIGUEZ E, BAYON R. Corrosion, wear and tribocorrosion performance of a thermally sprayed aluminum coating modified by plasma electrolytic oxidation technique for offshore submerged components protection [J]. Corrosion Science, 2018, 143: 258−280.

[29] CHAMPAGNE V K, HELFRITCH D, LEYMAN P, AHL S G, KLOTZ B. Interface material mixing formed by the deposition of copper on aluminum by means of the cold spray process [J]. Journal of Thermal Spray Technology, 2005, 14: 330−334.

[30] LU Hai-yang, SHANG Jian-tong, JIA Xiu-jie, LI Yan-le, LI Fang-yi, LI Jian-feng, NIE Yan-yan. Erosion and corrosion behavior of shrouded plasma sprayed Cr_3C_2−NiCr coating [J]. Surface & Coatings Technology, 2020, 388: 125534.

[31] NI Yu-meng, ZHANG Fan, NJOKU D I, YU Ying-jie, PAN Jin-shan, MENG Mei-jiang, LI Ying. Corrosion mechanism of CuAl−NiC abradable seal coating system-The influence of porosity, multiphase, and multilayer structure on the corrosion failure [J]. Journal of Materials Science & Technology, 2021, 88: 258−269.

[32] LEE H S, SINGH J K, PARK J H. Pore blocking characteristics of corrosion products formed on Aluminum coating produced by arc thermal metal spray process in 3.5 wt.% NaCl solution [J]. Construction and Building Materials, 2016, 113: 905−916.

基于冷喷涂工艺的 Mg−Zn−Al−Sn−Mn 合金防腐 Al 涂层制备

陈 良，鲍意浩，李志刚，钱丽华，赵国群，张存生

山东大学 材料液固结构演变与加工教育部重点实验室，济南 250061

摘　要：采用冷喷涂技术在 Mg−Zn−Al−Sn−Mn 合金表面制备 Al 涂层，以提高其耐腐蚀性能。研究工作气体温度和压力对 Al 涂层显微组织和腐蚀行为的影响。结果表明，随着气体温度和压力的升高，Al 涂层的致密度和厚度均明显增加。高的气体温度能降低颗粒沉积的临界速度，并提高沉积效率。高的气体压力不仅提升机械结合质量，而且对沉积的涂层具有较强的夯实作用。由于孔隙的减少，Al 涂层的耐蚀性随着气体温度和压力的升高而提高。$Al(OH)_3$ 和 Al_2O_3 等腐蚀产物可以堵塞涂层中的孔隙，并作为阻碍腐蚀的物理屏障，从而有效保护 Mg 合金免受腐蚀。

关键词：冷喷涂；镁合金；铝涂层；耐蚀性；显微组织

(Edited by Bing YANG)